EPJ B
Condensed Matter and Complex Systems
www.epj.org

Eur. Phys. J. B **66**, 419–426 (2008) DOI: 10.1140/epjb/e2008-00444-x

Two-phase flow model for energetic proton beam induced pressure waves in mercury target systems in the planned European Spallation Source

I.F. Barna, A.R. Imre, L. Rosta and F. Mezei

EDP SCIENCES
Società Italiana di Fisica
Springer

Eur. Phys. J. B **66**, 419–426 (2008)
DOI: 10.1140/epjb/e2008-00444-x

THE EUROPEAN PHYSICAL JOURNAL B

Two-phase flow model for energetic proton beam induced pressure waves in mercury target systems in the planned European Spallation Source

I.F. Barna[1,a], A.R. Imre[1], L. Rosta[2], and F. Mezei[2]

[1] KFKI Atomic Energy Research Institute (AEKI) of the Hungarian Academy of Sciences, P.O. Box 49, 1525 Budapest, Hungary
[2] Research Institute for Solid State Physics and Optics of the Hungarian Academy of Sciences, P.O. Box 49, 1525 Budapest, Hungary

Received 9 May 2008 / Received in final form 23 September 2008
Published online 9 December 2008 –

Abstract. Two-phase flow calculations are presented to investigate the thermo-hydraulical effects of the interaction between 2 ms long 1.3 GeV proton pulses with a closed mercury loop which can be considered as a model system of the target of the planned European Spallation Source (ESS) facility. The two-fluid model consists of six first-order partial differential equations that present one dimensional mass, momentum and energy balances for mercury vapor and liquid phases are capable to describe quick transients like cavitation effects or shock waves. The absorption of the proton beam is represented as instantaneous heat source in the energy balance equations. Densities and internal energies of the mercury liquid-vapor system is calculated from the van der Waals equation, but general method how to obtain such properties using arbitrary equation of state is also presented. A second order accurate high-resolution shock-capturing numerical scheme is applied with different kind of limiters in the numerical calculations. Our analysis show that even 75 degree temperature heat shocks cannot cause considerable cavitation effects in mercury.

PACS. 47.55.Kf Particle-laden flows – 47.90.a+ Other topics in fluid dynamics – 47.55.dp Cavitation and boiling

1 Introduction

A well-known non-destructive material research method is neutron scattering. Free neutrons for neutron beams for research purposes need to be extracted from their bound states of atomic nuclei. Energetic neutron beams can be produced in fission of heavy elements (e.g. ^{235}U) or by spallation. In fission of ^{235}U 190 MeV heat is released for each extracted fast neutron while in the spallation process only about 30 MeV heat is deposited per fast neutron. The deposited heat has to be removed by cooling and it ultimately becomes a limiting thermodynamic factor for the amount of neutrons produced. As a second distinct advantage of pulsed spallation sources over continuous ones is that a larger part of the neutrons produced can be delivered to the sample in monochromatic beams. These two advantages of spallation sources make it possible to construct more powerful neutron sources with larger neutron flux than ever before. The simple goal of the planned European Spallation Source (ESS) is to provide Europe with the most powerful neutron facility. A choice of a 5 MW proton beam power at 1.3 GeV proton energy with 111 mA proton beam current and with 16.66 Hz repetition rate of 2 ms long neutron pulses will produce an average thermal neutron flux density of 3.1×10^{14} n/cm^2 s in the ESS mercury target. A detailed analysis of the planned ESS can be found elsewhere [1]. This sudden proton pulse causes a thermal and a pressure shock in the target which may cause cavitation or tensile stress.

The question of cavitation erosion [2] has crucial importance in the constructional planning of any spallation neutron source target facility. Research groups in Japan and in the United States performed various experimental (both in-beam and off-beam) and theoretical investigations [3,4] to overcome this difficulty.

In the following study we present and analyze a one dimensional six-equation two-fluid model which is capable to describe transients like pressure waves, quick evaporation or condensation which is proportional to cavitation caused by energetic proton interaction in mercury target.

Our model has a delicate numerical scheme and capable to capture shock waves and describe transient waves

[a] e-mail: barnai@sunserv.kfki.hu

which may propagate quicker than the local speed of sound [5]. Most of the two-phase models have numerical methods which describes usual flow velocities much below the sonic conditions.

Our model can successfully reproduce the experimental data of different one- or two-phase flow problems such as ideal gas Riemann problem, critical flow of ideal gas in convergent-divergent nozzle, column separation or cavitation induced water hammer, rapid depressurization of hot liquid from horizontal pipes or even steam condensation induced water hammer [6].

According to our knowledge there is no real two-phase flow calculation for mercury flow system. Some timorous attempts were presented with the help of some commercial three dimensional industrial codes like Fluent or ANSYS [7,8] but the results are questionable. Some results show complete and immediate vaporization during the first proton pulse, which is contradictory to experimental observations. In our results chapter we analyse the cavitation model of Ida et al. [3] and the static model of Riemer [4] which – in our interpretation – is only useful for sudden heat shocks.

There are some study for three dimensional numerical simulation of magnetohydrodynamic processes in the muon collider mercury target. These studies takes strong external magnetic fields into account [9] but consider single phase only neglecting evaporization or condensations. The liquid phase of mercury was modeled using the stiffened politropic equation of state and the vapor phase was considered to be ideal gas. There is a literature survey on various fluid flow data for mercury from the politropic equation state [10] which can be directly applied in calculations. There are also different equation of states (EOS) available for mercury from microscopic molecular simulation [11,12] of from macroscopic theories like virial expansion [13] or from generalized van der Waals equation like the Redlich-Kwong equation [14] or the like [15]. Thermodynamical and flow properties of other liquid metals are also in the focus of recent scientific interest [14,16].

In the next sections we introduce our applied model, give a detailed analysis about phase transitions and present our pressure wave results with comparison to other studies [3,4].

2 Theory

2.1 Theory of two-phase flow

There is a large number of different two-phase flow models with different levels of complexity [17,18] which are all based on gas dynamics and shock-wave theory. In the following we present our one dimensional six-equation equal-pressure two-fluid model. The density, momentum and energy balance equations for both phases are the following:

$$\frac{\partial A(1-\alpha)\rho_l}{\partial t} + \frac{\partial A(1-\alpha)\rho_l(v_l-w)}{\partial x} = -A\Gamma_g, \quad (1)$$

$$\frac{\partial A\alpha\rho_g}{\partial t} + \frac{\partial A\alpha\rho_g(v_g-w)}{\partial x} = A\Gamma_g, \quad (2)$$

$$\frac{\partial A(1-\alpha)\rho_l v_l}{\partial t} + \frac{\partial A(1-\alpha)\rho_l v_l(v_l-w)}{\partial x} + A(1-\alpha)\frac{\partial p}{\partial x} - A\,CVM - Ap_i\frac{\partial \alpha}{\partial x} = AC_i|v_r|v_r - A\Gamma_g v_i + A(1-\alpha)\rho_l\cos\theta - AF_{l,wall}, \quad (3)$$

$$\frac{\partial A\alpha\rho_g v_g}{\partial t} + \frac{\partial A\alpha\rho_g v_g(v_l-w)}{\partial x} + A\alpha\frac{\partial p}{\partial x} + A\,CVM + Ap_i\frac{\partial \alpha}{\partial x} = -AC_i|v_r|v_r + A\Gamma_g v_i + A\alpha\rho_g\cos\theta - AF_{g,wall}, \quad (4)$$

$$\frac{\partial A(1-\alpha)\rho_l e_l}{\partial t} + \frac{\partial A(1-\alpha)\rho_l e_l(v_l-w)}{\partial x} + p\frac{\partial A(1-\alpha)}{\partial t} + \frac{\partial A(1-\alpha)p(v_l-w)}{\partial x} = AQ_{il} - A\Gamma_g(h_l + v_l^2/2) + A(1-\alpha)\rho_l v_l g\cos\theta + E_{l,pulse}(x,t), \quad (5)$$

$$\frac{\partial A\alpha\rho_g e_g}{\partial t} + \frac{\partial A\alpha\rho_g e_g(v_l-w)}{\partial x} + p\frac{\partial A\alpha}{\partial t} + \frac{\partial A\alpha p(v_l-w)}{\partial x} = AQ_{ig} + A\Gamma_g(h_g + v_g^2/2) + A\alpha\rho_g v_g g\cos\theta + E_{g,pulse}(x,t), \quad (6)$$

Index l refers to the liquid phase and index g to the gas phase. Nomenclature and variables are described in Table 1. Left hand side of the equations contain the terms with temporal and spatial derivatives. Hyperbolicity of the equation system is ensured with the virtual mass term CVM and with the inter-facial term (terms with p_i). Terms on the right hand side are terms describing the inter-phase heat, mass(terms with Γ_g vapor generation rate) volumetric heat fluxes Q_{ig}, momentum transfer (terms with C_i), wall friction F_{g_wall}, and gravity terms. A detailed analysis of the source terms can be found in [6]. There are different kind of inter-phase mass, heat and momentum transfer models exist for different flow regimes like disperse or horizontally stratified flows. These are the so called correlations. For inter-phase momentum and mass transfer we use the standard correlations used for water. However, for fluid heat transfer we changed the applied correlation [6]

$$Nu = \max[4, (1/8 f_k(Re-1000)Pr)/(1+12.7\sqrt{f_k/8} \times(Pr^{0.67}-1))] \quad (7)$$

to the Subbotin [19] correlation

$$Nu = 7 + 0.025Pe^{0.8}, \quad (8)$$

which is well established for liquid metals. Where Nu is the Nusselt, Pr is the Prandt, Re is the Reynolds and Pe is the Péclet number, f_k is the heat diffusivity. Unfortunately, there are no more correlations (like bubble drag coefficients) known for mercury.

Table 1. Nomenclature used in the two-phase flow equations (Eqs. (1–6)).

A pipe cross section (m^2)
C_i internal friction coefficient (kg/m^4)
CVM virtual mass term (N/m^3)
e_i specific total energy ($e = u + v^2/2$) (J/kg)
$F_{i,wall}$ wall friction per unit volume (N/m^3)
g gravitational acceleration (m/s^2)
h_i specific enthalpy ($h = u + p/\rho$) (J/kg)
p pressure (Pa)
p_i interfacial pressure $p_i = p\alpha(1-\alpha)$ (Pa)
Q_{ig} interf.-liq./gas heat transf. per vol. rate (W/m^3)
t time (s)
u_i specific internal energy (J/kg)
v_i velocity (m/s)
v_r relative velocity ($v_r = v_g - v_l$) (m/s)
w pipe velocity in flow direction (m/s)
x spatial coordinate (m)
Γ vapor generation rate (kg/m^3)
α vapor void fraction
ρ_i density (kg/m^3)
θ pipe inclination

The last term in the energy equations $E_{i,pulse}(x,t)$ represents the deposited energy from the proton beam and will be specified later on.

Two additional equation of states (EOS) are needed to close the system of equations (Eqs. (1–6))

$$\rho_k = \left(\frac{\partial \rho_k}{\partial p}\right)_{u_k} dp + \left(\frac{\partial \rho_k}{\partial u_k}\right)_p du_k. \tag{9}$$

Partial derivatives in equation (9) are expressed using pressure and specific internal energy as an input. In the following we show how the liquid-steam table – a sixfold numerical table – $(p, T, \rho_l, u_l, \rho_g, u_g)$ can be created for mercury from an arbitrary EOS. To avoid technical difficulties we do not modify (Eqs. (1–6)) including the used analytic EOS, just create a numerical liquid-steam table. In this manner arbitrary two phase-flow systems can be investigated with the same model in the future (e.g. lead-bismuth eutectic, liquid Li or He). Liquid metal systems can operate on low (some bar) pressure and have larger heat conductivity than water which can radically enhance thermal efficiency.

We start with the usually parameterized van der Waals EOS from

$$p = \frac{RT}{V-b} - \frac{a}{V^2} \tag{10}$$

where $R = 8.314$ J/mol/K is the universal gas constant and parameters a and b are related with the critical molar volume (V_c) temperature (T_c) and pressure (p_c) of the considered fluid: $a = 9P_cV_c^2$, $b = V_c/3$. For the critical temperature and pressure of Hg the $T_C = 1733 \pm 50$ K and $p_C = 160.8 \pm 5$ MPa data were taken from [14]. T, p and V are the temperature, pressure and the volume, respectively. (We just mention that in [14] the parameter a is given wrong.) The fluid density with the corresponding saturated vapor density can be easily determined from the EOS with the well-known Maxwell construction. To obtain the internal energies for both phases is a bit more difficult task. We start with the second law of thermodynamics

$$du = Tds - pdV \tag{11}$$

where s is the entropy and u is the internal energy. With the Maxwell relations $\left(\frac{\partial T}{\partial V}\right)_s = -\left(\frac{\partial P}{\partial s}\right)_V$ we end up with the following working equation

$$du = c_V dT + \left[T\left(\frac{\partial p}{\partial T}\right)_V - p\right] dV. \tag{12}$$

The internal energy is a thermodynamical potential therefore the choice of the zero point can be defined arbitrary, we took $T = 253.14$ K which is 10 degree above the melting point of solid mercury at normal pressure. The heat capacity at constant volume c_v may in turn be calculated from the heat capacity at constant pressure $c_p$with the thermodynamic relation

$$c_p = c_V + T\left(\frac{\partial V}{\partial T}\right)_p^2 \left(\frac{\partial p}{\partial V}\right)_T \tag{13}$$

where $\frac{1}{V}\frac{\partial V}{\partial T} = \alpha_T$ is the thermal expansion coefficient. To avoid further misunderstanding in this study we use α_T for the thermal expansion coefficient and α for vapor void fraction. Polynomial fits for the temperature dependence of experimental data of heat capacity c_p and expansion coefficient α_T [20](or [10]) help us to calculate the internal energy of the liquid state. Finally, the internal energy of the corresponding gas phase has to be determined. In the temperature range of 270–500 K (which is our recent interest) the experimental data of the vaporization heat [12] can be satisfactory fitted with a linear function. With this method a two-phase liquid-steam table was constructed between 270–500 K and 7 to 7×10^7 Pascal pressure. There is only one negative pressure value given for each temperature in our table. Unfortunately, our physical and numerical method cannot calculate hydrodynamics with negative pressure. If the pressure of the system falls below zero than a sudden boiling is started until the pressure becomes positive.

Additional flow properties of mercury like dynamic viscosity and heat transfer coefficients are approximated with piecewise continuous temperature dependent functions from [10]. The surface tension was considered as a linear function of temperature [21].

The effect of the 1.3 GeV proton pulse was treated as a sudden thermal shock which means an additional source term in both energy equations $E_{i,pulse}(x,t)$. The deposited energy of the proton beam in the mercury target is proportional to the density. With the introduction of the mixture density $\rho_m = \alpha\rho_g + (1-\alpha)\rho_l$ the interaction between the proton-mercury two-phase flow can be further improved.

According to experimental proton beam analysis the spatial energy distribution of the beam along the propagation direction of the mercury flow has a parabolic shape [22,23] with a diameter of 20 cm. The presented flow model is one dimensional, hence there is no room to include radial energy deposition distribution inside the mercury. To describe well-defined finite duration we use $\sin^2$ envelope with $\tau = 2$ ms pulse length.

$$E_{g,pulse}(x,t) = \frac{\rho_g \alpha}{\rho_m} E_0 \sin^2\left(\frac{\pi t}{\tau}\right)(1-(x/x_s)^2) \tag{14}$$

$$E_{l,pulse}(x,t) = \frac{\rho_l (1-\alpha)}{\rho_m} E_0 \sin^2\left(\frac{\pi t}{\tau}\right)(1-(x/x_s)^2). \tag{15}$$

Ida et al. [3] consider an idealized external driving pressure with a trapezoidal time shape. The effective range of 1.3 GeV protons in mercury can be calculated with the Bragg theory and gives 41 cm [24]. An accurate 3 dimensional absorbed proton energy distribution in the target can be used as an input in commercial flow codes like Fluent but the results like the pressure waves still remain questionable. Experimental consideration state that 47% of the original 5 MW beam power is absorbed in the target which is 2.35 MW. In the planned ESS facility a train of 16.66 proton pulses will come with 2 ms long pulse duration and the total sum of these pulses give the 5 MW beam power. Hence, the peak power parameter E_0 has to be normalized in such a way that the spatial and time integral of $E_{i,pulse}(x,t)$ gives the absorbed 2.37 MW power of the original 5 MW beam.

The system of equations (1–6) represents the conservation laws and can be formulated in the following vectorial form

$$\mathbf{A}\frac{\partial \boldsymbol{\Psi}}{\partial t} + \mathbf{B}\frac{\partial \boldsymbol{\Psi}}{\partial x} = \boldsymbol{S} \tag{16}$$

where $\boldsymbol{\Psi}$ represents the vector of the independent nonconservative variables $\boldsymbol{\Psi}(p, \alpha, v_l, v_g, u_l, u_g)$, $\mathbf{A}$ and $\mathbf{B}$ are the matrices of the system and $\boldsymbol{S}$ is the source vector of non-differential terms. These three quantities $\mathbf{A}$, $\mathbf{B}$ and $\boldsymbol{S}$ can be obtained from equations (1–6) with some algebraic manipulation. In this case the system eigenvalues which represent wave propagation velocities are given by the determinant $\det(\mathbf{B} - \lambda\mathbf{A})$. An improved characteristic upwind discretization method is used to solve the hyperbolic equation system (16). The problem is solved with the combination of the first- and second-order accurate discretization scheme by the so-called flux limiters to avoid numerical dissipation and unwanted oscillations which appear in the vicinity of the non-smooth solutions. Exhaustive details about the numerical scheme can be found in [5,6].

2.2 Liquid-vapor phase transition in the meta-stable region

Water boils at 100 °C (373.15 K) under atmospheric pressure; this is a well-known, but not entirely correct piece of the common knowledge. Boiling is usually defined (at least phenomenologically) when liquid-vapor phase transition happens not only at the already existing interfaces, but within the bulk liquid too. For water, it happens usually at the already mentioned 100 °C, but not always. Overheating of liquids is a phenomenon known for every chemistry students; you can exceed the boiling point with a few degrees, without getting boiling, but then it can happen suddenly, exploding the whole amount of liquid (and often the container too) [25]. In the following, we are going to explain this phenomenon and show its importance in the cavitation of mercury. Liquid can co-exists with the vapor of the same material, without any problem. The conditions (temperature and pressure) where they co-exist are described the vapor pressure curve (also called saturation or co-existence curve). Liquid and vapor states can be described by equation of states (EOS); like van der Waals EOS. A schematic isotherm (describing pressure and volume on a constant temperature) can be seen in Figure 1a. The isotherm has two extrema (marked as B and D), these are the so-called spinodal points (liquid-vapor and vapor-liquid; LV and VL spinodals). Between the two spinodals, the system would be unstable, due to the negative compressibility, therefore these states (the ones on the curve between points B and D) cannot exist. The equilibrium conditions can be calculated by using the Maxwell construction: a line (parallel to the V-axis) has to be drawn in a way that the area between the isotherm and the Maxwell-line between points A and C and C and E has to be equal. Then the intersects (A and E) gives the co-existing liquid and vapor volumes (or densities) and the equilibrium pressure on the given temperature. Plotting the pressures on different temperatures, one would obtain the vapor pressure curve, like the solid line in Figure 1b. It can be seen that points A and E are not special points of the isotherm. The liquid is not forced to boil at point A; it would be forced only at point B (where liquid phase

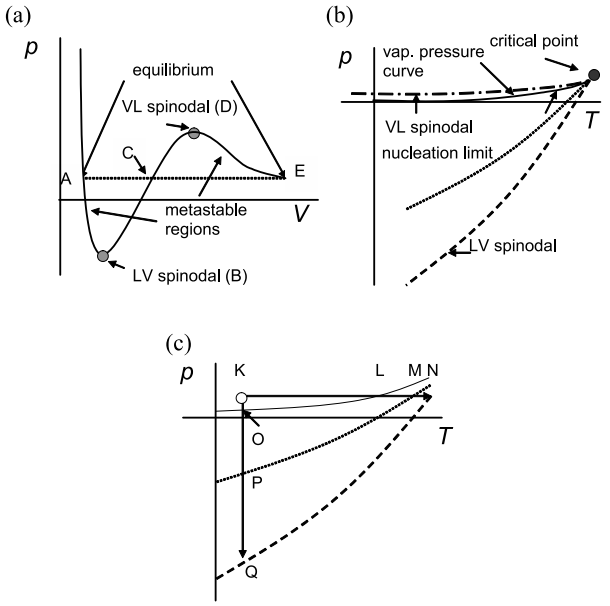

Fig. 1. (a) A sub-critical isotherm of a van der Waals type fluid. (b), (c) Related stability lines (see text).

cannot exists any more). Plotting Bs at different temperature, one would obtain the so-called liquid-vapor spinodal (dashed line in Fig. 1b), the stability limit of liquid state. The vapor-liquid spinodal (dot-dash line in Fig. 1b) is important when we have over-saturated vapor; we are going to neglect it here. The AB and DE parts on the isotherm are meta-stable; in Figure 1b these parts are represented by the region between the vapor pressure curve and the LV spinodal. Liquid (without co-existing vapor phase) can exist in this region; even can exist under negative pressure [25,26] The real boiling happens in this meta-stable region. Close to the vapor pressure curve the liquid is only slightly meta-stable, can live for long time without nucleating vapor bubbles; far away from it (close to the spinodal) the liquid will be very meta-stable and cavitate (boil) with higher probability. The bubble nucleation can happen in two different ways. The heterogeneous nucleation happens when the liquid already has a nucleus, usually a tiny bubble hidden in a crevice of the wall or stuck onto a floating particle. Due to the small size (i.e. high curvature) the micro-bubble can be in equilibrium with a meta-stable liquid for a while, but when the temperature is too high or the pressure is too low, it will initiate boiling. The other process is the homogeneous nucleation. In that case, the initial micro-bubble will be produced by the density fluctuations of the liquid; when the fluctuation is big enough to call it "bubble", then it will initiate the boiling. In everyday life, boiling happens by heterogeneous nucleation, practically in the immediate vicinity of the vapor pressure curve. In clean liquids (like distilled water) the boiling can happen much farther. It is a well-known practice to avoid overheating (and the explosion-like boiling, following it) to put some bubble seed into the liquid, like a few pieces of sponge-like pumice (or boiling-) stones. In these nucleation processes – especially in homogeneous nucleation – time is also an important factor; a liquid can endure high overheating/stretching for a small period of time [25–28]. Therefore one cannot draw a well-defined line as nucleation limit onto the phase diagram (Fig. 1b, c); the dotted line drawn by us is only for demonstration. The exact location depends on the purity of liquid, the amount of external disturbances (even cosmic rays can generate bubbles in meta-stable liquids) and – in a great extent – on the time scale. In Figure 1c, a magnified part of Figure 1b (without the VL spinodal, which is irrelevant in our case) can be seen. K marks a state, where the liquid is in stable liquid phase; there is no vapor phase present. To obtain phase transition, the temperature has to be increased or the pressure has to be decreased. By increasing the temperature (and keeping a constant pressure), the vapor pressure curve will be reached at point L. This is the first point, where the liquid can boil and vapor phase might appear, but in clear and undisturbed liquid, the probability of boiling here is very small. Increasing the temperature further, the nucleation limit will be reached (point M); here the phase transition will surely happen, due to heterogeneous or homogeneous nucleation, forming initially small, but continuously growing separated bubbles, which later can merge into a continuous vapor phase. When the liquid is perfectly clean, all disturbances are suppressed and the heating is very fast, etc., then this nucleation limit can be pushed very close to spinodal limit (point N), where liquid phase cannot exist any more. When the phase transition happens at the spinodal limit, one will obtain two bi-continuous phases (liquid and vapor), instead of a continuous (liquid) and an separated (vapor bubbles) one, obtained during nucleation. We should remark, that for the first appearance of the vapor phase, the system will jump back to the vapor pressure curve (which will be detected as a pressure jump). Changing the pressure at constant temperature, one would reach the vapor pressure curve at point O, then the nucleation limit at point P, finally the spinodal limit at point Q, with the same results as is happen with temperature increase. To see the extent of the effect, we will give numerical examples for water and for mercury. For water, starting from room temperature (293.15 K, 1 bar), we will reach the vapor pressure curve 373.15 K. Increasing the temperature, boiling might happen any time; the highest experimentally obtained value for overheating (i.e. point M) was around 570 K [30] giving almost 200 K overheat. The spinodal temperature for water on atmospheric pressure is still debated, is has to be located above the previously mentioned overheating limit, but certainly below the critical temperature. Also for water, by decreasing the pressure, the vapor pressure curve (point O) would be reached at 0.025 bar pressure. The experimental limit of stretching is –1200 bar [30], where the estimated spinodal (depending on the model) is between –2000 and –4000 bar. For mercury at 7 bar (which is the working pressure for the mercury in the ESS) the boiling point is at 760 K, it is very far from the working temperature (which is room temperature, 300 K). The limit of overheating is not known, but surely below the critical temperature, which is around 1700 K. Concerning pressure drop, the vapor pressure of mercury is almost zero (less than 2×10^{-6} bar); concerning the fact that the working pressure is 7 bar, the possibility of a pressure drop of this extent is very improbable. The measured nucleation limit of mercury at room temperature is in the –2 to −425 bar range [29]; therefore to get bubbles, the pressure should drop from +7 bar to −2 bar for a longer period. The absolute (spinodal) limit is unknown. Although in the ESS, pressure decrease and temperature increase happens simultaneously, the working conditions are so far from the beginning of the boiling region (vapor pressure curve) that the possibility to reach it is negligible, except under special circumstances. First, there is a possibility for fast pressure oscillation after the proton pulse; the amplitude can be even 300 bar [32], which would be enough to cause cavitation. The other scenario would require gas-contamination (pre-existing gas bubbles in the mercury); in that case even a tiny pressure decrease or temperature increase can cause the growing of these micro-bubbles, mimicking boiling [32]. Non-uniform temperature and pressure distribution can cause shear stresses, which can also cause cavitation in the liquid. Finally, the proton beam itself can initiate cavitation, but only when the meta-stable states are already reached.

We can conclude, that with a few bar pressure drop and a few tens of K temperature increase, the cavitation in the pure mercury target has low possibility. On the other hand, concerning the reported cases of cavitation in similar facilities [31] indicate, that either the conditions (T, p) might change more drastically or some phenomena, neglected by us (like pressure oscillation, shear stresses, etc.) can play more important role.

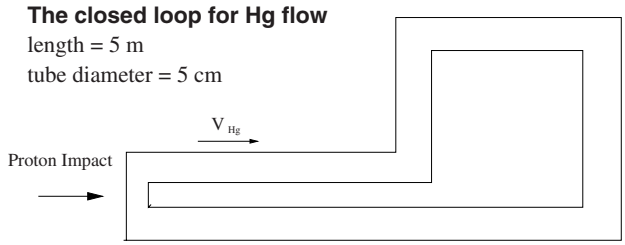

Fig. 2. The schematic geometrical model of the ESS target.

3 Results and discussion

The ESS mercury target loop is a complex facility with various pumps, heat exchangers and tanks [1]. We model however with a simple six-sided closed loop (see Fig. 2) of a pipe with diameter of 5 cm and total length of 5 m. Although our model is less detailed than the real loop but topologically equivalent and geometrically similar. Any closed loop model is capable to describe the propagation of the shock and rarefraction waves of the "two-sided Riemann problem". In the original Riemann problem a membrane divides the shock tube into two distinct parts, where the pressure and temperature are different. At $t = 0$ time point the membrane is removed and a shock and rerefraction wave is formed which began to propagate in opposite directions. In our ESS model the closed mercury loop is divided into two different parts. The left side, (the vertical pipe) of Figure 2 has $T = 375$ K temperature and the rest of the loop has $T = 300$ K. In this sense two interfaces, two 300–370 K non-continous temperature steps formed in the loop. These two interfaces are the source of two independent shock and rarefraction waves ("two-sided Riemann problem") which will propagate and interact in the tube later on. The original temperature of the mercury is $T = 300$ K with pressure of 7 bar and flow velocity of $v = 4.6$ m/s. The proton beam interacts with a mercury via a 20×5 cm^2 window. A simple calculation shows that 84 375 J of energy will heat up 10 kg of mercury with a $\Delta t = 75$ K. We applied a single pulse shot at time equal to zero and integrated the two-phase flow equations (16) up to $t_{max} = 10^{-2}$ s. A second order numerical scheme was used with the MINMOD flux limiter [5]. The Courant number which measures the relative wave propagation speeds of the exact solution and the numerical solutions was set to $CFL = 0.6$. The pressure history at the beam-target interaction point is presented in Figure 3. After the initial pulse at $t = 1.6$ ms the pressure reaches its maximal value which is 50% higher than the original pressure. The speed of sound in mercury is 1451.4 m/s at 293 K. The length of our closed loop was set to 5 m. The time delay between the pressure peaks coming one after another is about $\tau = 5$ m/1451 m/s = 0.0034 s which means that there are 3 peaks in a 0.01 s time interval. This can be clearly seen in the figure. At the left shoulder of the first four pressure peaks we can see the decay of the rarefraction waves. Detailed analysis showed us that the two shock and the two rarefraction waves interact after the proton pulse giving us the above presented pressure pattern. It is well-known from shock

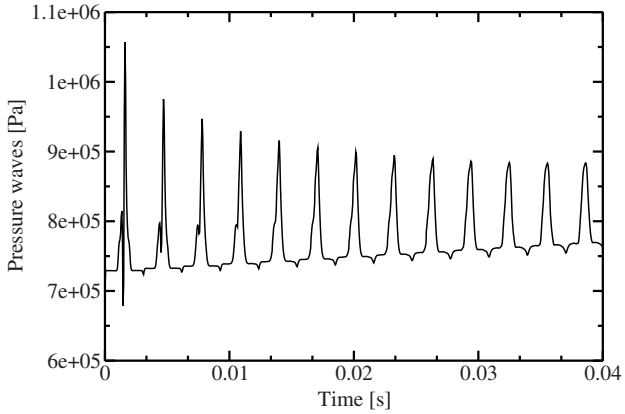

Fig. 3. Time history of pressure at the point of the proton impact.

wave theory [33] that there is a $1/\sqrt{t}$ time decay of the shock wave amplitudes for ideal gas even without any internal friction. Such a decay can be seen also in Figure 3. An additional complementary physical effect is the slowly enhancing static pressure of mercury between the overpressure peaks which is a numerical proof of the energy and momentum conservation.

After the pulse the pressure does not fall below the initial pressure and the temperature will cool down to 300 K. The mercury vapor void fraction was originally set to zero ($\alpha = 10^{-12}$) which did not change during the time propagation allowing only "nanobubbles", too small to act as cavitation nuclei. If we consider one or two percent initial vapor void fraction (as a model for small bubbles) than a quick condensation can be observed. Numerous tests showed that a given initial vapor void fraction can not be enhanced in such kind of mercury flows, where the flow velocity is in the magnitude of some m/s, the liquid temperature is close to room temperature and the initial pressure is about 7 bar. If we apply an elastic pipe with an elasticity of 2×10^{11} N/m^2 Young's modulus (which are usual for steel) or/and include or exclude any kind of additional wall friction [6] for the fluid the pressure peaks will not be changed. The maximum difference was about 6%. There is a strong indication that mercury is a non-wetting fluid on steel surface so the wall friction is negligible during the simulation.

There are two models available in the recent literature which try to prognosticate the maximal pressure in

ESS mercury targets or try to predict cavitation. The first one is from Riemer [4] which is valid for a static Hg volume bombarded with a sudden thermal energy shock. The maximal pressure is

$$dP = \frac{Q\beta K}{\rho C_v} \tag{17}$$

where dP is the maximal pressure (Pa), Q is the deposited energy per volume (J/m^3), β is the volumetric expansion coefficient (183×10^{-6} K), K is the mercury bulk modulus of elasticity (28.6 GPa), ρ is the density (13 500 kg/m^3) and C_v is the constant volume specific heat of Hg (140 J/kg K). This model is valid if we completely neglect hydrodynamics and consider that the force calculated from thermal expansion is equal with the force of elastic compressibility coming from outside. Which means complete volume conservation of mercury. This model predicates about many hundred bars for the ESS target, depending on the deposited energy per volume element. Our model, however gives a much smaller pressure peak, because of the proton beam pulse interacts with a moving mercury target, and the Q value is much smaller. Another condition is that the real container of the ESS target is elastic and let mercury to expand. The second model, which is much more complex and try to investigate the caviation problem in spallation targets was developed by Ida et al. [3]. As a first step they performed experimental studies using a magnetically driven impact test device, called MIMTM (Magnetic Impact Testing Machine) and generated compressive mechanical impacts of an input power of 560 W on mercury causing overpressure peaks with an approximate magnitude of 4.4 bar. They directly observed cavitation bubbles in mercury. With this initial pressure values they used the Rayleigh-Plesset single-bubble theory which takes into account bubble-wall and additional effective bubble-bubble interactions to explain the growth rates of bubbles. However, there are discrepancies between the experimental and theoretical data because evaporation or condensation effects were not taken into account. Their model also neglect hydrodynamical effects, namely consider a static bulk mercury. The condensation time for bubbles after the impact is about 2–3 ms.

4 Summary and outlook

With the help of a one dimensional two-phase flow model we calculated the pressure waves and vapor void fractions in mercury induced by energetic proton beams. Our analysis showed that no vapor bubbles or cavitation effects can be seen after the first absorbed proton pulse. Further, in depth analysis is in progress to investigate geometrical effects of the mercury target loop which is a complex facility with various pumps, heat exchangers and tanks [1]. Our model can include abrupt area changes, or convergent-divergent pipe cross section changes, or even heat exchangers. We model however with a simple six-sided closed loop (see Fig. 2) of a pipe with diameter of 5 cm and total length of 5 m. The original temperature of the mercury is $T = 300$ K with pressure of 7 bar and flow velocity of $v = 4.6$ m/s. The proton beam interacts with a mercury via a 20×5 cm^2 window. A simple calculation shows that 84 375 J of energy will heat up 10 kg of mercury with a $\Delta t = 75$ K. A single pulse shot at time equal to zero was applied and the equations (16) was solved upto $t_{max} = 10^{-2}$ s. A second order numerical scheme was used with the MINMOD flux limiter [5]. The Courant number was set to $CFL = 0.6$. The pressure history of the beam-target interaction point is presented in Figure 2. After the initial pulse at $t = 1.6$ ms the pressure reaches its maximal value which is 50% higher than the original pressure. After the pulse the pressure does not fall below the initial pressure and the temperature will cool down to 300 K. The mercury vapor void fraction was originally set to zero ($\alpha = 10^{-12}$) which did not changed during the time propagation allowing only "nanobubbles", too small to act as nucleus for cavitation. The question of the vapor void fraction, pipe elasticity or the liquid wall friction was examined also.

We would like to emphasize that further in-depth analysis are needed to clear up the question of a long pulse train. The question of different equation of states will be investigated also. As a long term interest we also planed to investigate other liquid metal (e.g. bismuth-lead eutectic or liquid lithium) or liquid helium systems which can be interesting as a cooling media for new type of nuclear reactors. Liquid metal systems can operate on low (some bar) pressure and have much larger heat conductivity than water which can radically enhance thermal efficiency.

References

1. The European Spallation Source Project, Technical Report, `http://neutron.neutron-eu.net/n_ess`
2. M. Futakawa, T. Naoe, C.C. Tsai, H. Kogawe, S. Ishikura, Y. Ikeda, H. Soyama, H.H. Date, Cavitation Erosion in Mercury Target of Spallation Neutron Source, *Fifth International Symposium on Cavitation (cav2003)*, Osaka, Japan, November 1–4, 2003
3. M. Ida, T. Naoe, M. Futukawa, Phys. Rev. E **75**, 046304 (2007); M. Ida, T. Naoe, M. Futukawa, Phys. Rev. E **76**, 046309 (2007)
4. B.W. Riemer, J. Nucl. Mat. **343**, 81 (2005)
5. I. Tiselj, S. Petelin, J. Fluid Eng. -TASME. **120**, 363 (1998)
6. I. Tiselj, A. Horvath, G. Cerne, J. Gale, I. Parzer, B. Mavko, M. Giot, J.M. Seynhaeve, B. Kucienska, H. Lemonnier, WAHA3 code manual, Deliverable D10 of the WAHALoads project, March 2004
7. 3rd High-Power Targetry Workshop, September 10–14, 2007 Bad Zurzach, Switzerland, `http://asq.web.psi.ch/hptrgts/index`
8. H. Kogawa, et al. J. Nucl. Mat. **34**, 3178 (2005)
9. R. Samuliak, *Numerical simulation of hydro- and magneto-hydrodynamical properties in the Muon Collider target, Lecture Notes in Comp. Sci.* (Springer-Verlag, Berlin Heidelberg New York, 2002), Vol. 2331, pp. 391–400

10. H. Cords, A Literature Survey on Fluid Data for Mercury – Constitutive Equation, `http://neutron.neutron-eu.net/n_ess`
11. H. Kitamura, J. Chem. Phys. **126**, 134509 (2007)
12. G. Raabe, R.J. Sadus, J. Chem. Phys. **119**, 6691 (2003)
13. N. Mehdipour, A. Bousheri, Int. J. Thermophys. **18**, 1329 (1997)
14. K. Morita, V. Sobolev, M. Flad, J. Nucl. Mat. **362**, 227–234 (2007)
15. M.M.Z. Martynyuk, Fiz. Khim. **65**, 1716 (1981)
16. N. Mehdipour, A. Boushehri, H. Eslami, J. Non-Cryst. Solids **351**, 1333 (2005)
17. H.B. Stewart, B. Wendroff, J. Comp. Phys. **56**, 363 (1984)
18. R. Menikoff, B. Plohr, Rev. Mod. Phys. **61**, 75 (1989)
19. V.L. Subbotin et al., Int. J. Heat Mass Transfer **4**, 79 (1961)
20. L.A. Davis, R.B. Gordon, J. Chem. Phys. **46**, 2650 (1967)
21. J.J. Jasper, Phys. Chem. Ref. Data **1**, 841 (1972)
22. L. Ni, G.S. Bauer, H. Spitzer, Nucl. Instr. Meth. Phys. Res. A **425**, 57 (1999)
23. M. Futakawa, K. Kikuchi, H. Conrad, H. Stechmesser, Nucl. Instr. Meth. Phys. Res. A **439**, 1 (2000)
24. J.F. Ziegler, J.P. Biersack, U. Littman, *The stopping and Ranges of Ions in Matter* (Pergamon Press, Oxford, 1985)
25. P.G. Debenedetti, *Metastable Liquids: Concepts and Principles* (Princeton University Press, Princeton, 1996)
26. D.H. Trevena, *Cavitation and Tension in Liquids* (Adam Hilger, Bristol, 1987)
27. A. Imre, K. Martinás, L.P.N. Rebelo, J. Non-Equilib. Thermodyn. **23**, 351 (1998)
28. *Liquids Under Negative Pressure*, edited by A.R. Imre, H.J. Maris, P.R. Williams (NATO Science Series, Kluwer, Dordrecht, 2002)
29. L.J. Briggs, J. Appl. Phys. **24**, 488 (1953)
30. Q. Zheng, D.J. Durben, G.H. Wolf, C.A. Angell, Science **254**, 829 (1991)
31. D. Hidefumi, M. Futakawa, Int. J. Impact Eng. **32**, 118 (2005)
32. R.P. Taleyarkhan, F. Moraga, Nucl. Eng. Des. **207**, 181 (2001)
33. J. Smoeller, *Shock Waves and Reaction-Diffusion Equations* (Springer Verlag, 1983)